

The cell polarity kinase Par1b/MARK2 activation selects specific NF- κ B transcripts via phosphorylation of core mediator Med17/TRAP80

Anastasia Mashukova^{a,b,†}, Radia Forteza^{a,†}, Viraj N. Shah^a, and Pedro J. Salas^{a,*}

^aDepartment of Cell Biology, University of Miami Miller School of Medicine, Miami, FL 33136; ^bDepartment of Medical Education, Dr. Kiran C. Patel College of Allopathic Medicine, Nova Southeastern University, Fort Lauderdale, FL 33314

ABSTRACT Par1b/MARK2 is a Ser/Thr kinase with pleiotropic effects that participates in the generation of apico-basal polarity in *Caenorhabditis elegans*. It is phosphorylated by atypical PKC(ι/λ) in Thr595 and inhibited. Because previous work showed a decrease in atypical protein kinase C (aPKC) activity under proinflammatory conditions, we analyzed the hypothesis that the resulting decrease in Thr595-MARK2 with increased kinase activity may also participate in innate immunity. We confirmed that pT595-MARK2 was decreased under inflammatory stimulation. The increase in MARK2 activity was verified by Par3 delocalization and rescue with a specific inhibitor. MARK2 overexpression significantly enhanced the transcriptional activity of NF- κ B for a subset of transcripts. It also resulted in phosphorylation of a single band (~Mr 80,000) coimmunoprecipitating with RelA, identified as Med17. In vitro phosphorylation showed direct phosphorylation of Med17 in Ser152 by recombinant MARK2. Expression of S152D-Med17 mimicked the effect of MARK2 activation on downstream transcriptional regulation, which was antagonized by S152A-Med17. The decrease in pThr595 phosphorylation was validated in aPKC-deficient mouse jejunal mucosae. The transcriptional effects were confirmed in transcriptome analysis and transcript enrichment determinations in cells expressing S152D-Med17. We conclude that the MARK2-Med17 axis represents a novel form of cross-talk between polarity signaling and transcriptional regulation including, but not restricted to, innate immunity responses.

Monitoring Editor

Keith Mostov
University of California,
San Francisco

Received: Oct 20, 2020

Revised: Jan 25, 2021

Accepted: Feb 10, 2021

This article was published online ahead of print in MBoC in Press (<http://www.molbiolcell.org/cgi/doi/10.1091/mbc.E20-10-0646>) on February 17, 2021.

[†]Equal contributions to this work.

*Address correspondence to: Pedro J. Salas (psalas@miami.edu).

Abbreviations used: aPKC, atypical protein kinase C; CRE, bacteriophage P1 recombinase; CXCL, C-X-C motif ligand chemokines; GAPDH, glyceraldehyde-3-phosphate Dehydrogenase; GFP, green fluorescent protein; IC50, inhibitor concentration blocking 50% activity; IgG, immunoglobulin G; IKK, I kappa beta kinase; IL, interleukin; KO, knockout; MARK, microtubule-affinity regulating kinase; MDCK, Madin-Darby canine kidney cells; Med, mediator complex subunit; NF- κ B, nuclear factor kappa beta; NS, not significant; Oe, overexpression; Par, partitioning defective phenotype; RelA, p65 subunit of NF- κ B; SN, supernatant; STK11, serine-threonine kinase 11; TNF α , tumor necrosis factor alpha; WB, western blot.

© 2021 Mashukova, Forteza, et al. This article is distributed by The American Society for Cell Biology under license from the author(s). Two months after publication it is available to the public under an Attribution-Noncommercial-Share Alike 3.0 Unported Creative Commons License (<http://creativecommons.org/licenses/by-nc-sa/3.0>).

"ASCB®," "The American Society for Cell Biology®," and "Molecular Biology of the Cell®" are registered trademarks of The American Society for Cell Biology.

INTRODUCTION

The products of genes involved in *Caenorhabditis elegans* embryo partition (Par) (Kemphues et al., 1988) and polarization (Macara, 2004) interact among themselves and with other polarity proteins to determine apical (luminal) and basolateral polarity in epithelial cells and are involved in the asymmetry of other cell types. Emblematically, the polarity complex aPKC (atypical protein kinase C, PKC ι/λ and ζ , Par6, and Par3) is localized to the apical side nearby tight junctions. aPKC phosphorylates the basolateral determinant Par1b (MARK2; microtubule-affinity regulating kinase) in Thr595, a modification that inhibits MARK2 activity and releases it from the membrane (Hurov et al., 2004; Suzuki et al., 2004). In turn, Par1b phosphorylates Par3 and releases it from the polarity complex. This phosphorylation results in Par3 broad cytoplasmic distribution of Par3 as opposed to junctional localization (Macara, 2004; Suzuki and Ohno, 2006).

Par1b (MARK2, Emk1) knockout or Par1a (MARK3, hereafter referred to by their MARK names) knockout mice are viable. MARK3-deficient animals show metabolic phenotypes with changes in adiposity and glucose tolerance (Lennerz *et al.*, 2010). MARK2 null mice, in addition, show alterations of hypophyseal hormones (Bessone *et al.*, 1999) and immune system dysfunction and inflammation (Hurov *et al.*, 2001). The double knockout mouse is embryonic lethal (Lennerz *et al.*, 2010), but to our knowledge, there are no published data showing the phenotype leading to embryo death. In humans, splice variants of MARK2 were found associated to increased inflammation in renal grafts, but the mechanism remains elusive (Hueso *et al.*, 2004). In cancer cells, MARK2 is related to various transcriptional pathways including innate immunity NF- κ B (nuclear factor kappa B [Hubaux *et al.*, 2015]). In MDCK (Madin–Darby canine kidney) cells, MARK2 induces the formation of lateral lumens, resembling polarity in hepatocytes (Cohen *et al.*, 2004). It phosphorylates microtubule-associated proteins and influences microtubule organization (Sato *et al.*, 2013). It also has an effect in liver lipogenesis (Kim *et al.*, 2015). Interestingly, it has been shown to regulate the Wnt signaling pathway, thus possibly regulating downstream transcriptional activity (Elbert *et al.*, 2006). In addition, MARK2 also regulates class II histone deacetylases (Dequiedt *et al.*, 2006). In summary, the pleiotropic effects of MARK2 phosphorylations may be characterized as cytoplasmic (such as phosphorylation of Par3 or microtubules) or genomic (e.g., effects on the Wnt pathway or histone deacetylases). The latter are potentially more consequential to the overall cellular behavior, considering that they affect the expression of a broad range of proteins.

Epithelial polarity and innate immunity have coevolved in metazoans (Gilmore and Wolenski, 2012; Ganot *et al.*, 2015; Salinas-Saavedra *et al.*, 2015). In fact, it is broadly accepted that activation of the NF- κ B and interferon (IFN) pathways down-regulate lateral junctions, cell–cell adhesion, and increases epithelial permeability (Koch and Nusrat, 2012; Capaldo *et al.*, 2014; Garcia-Hernandez *et al.*, 2017). These effects are, to a large extent, caused by expression of myosin light chain kinase (MLCK) under NF- κ B transcriptional regulation (Capaldo and Nusrat, 2009; Lorentz *et al.*, 2017; Nighot *et al.*, 2019). Our lab made the intriguing observation that under NF- κ B/IFN stimulation by extracellular TNF α (tumor necrosis factor) and IFN γ , intestinal epithelial cells posttranslationally down-regulate aPKC (Mashukova *et al.*, 2011; Forteza *et al.*, 2016). This effect was observed in a model of intestinal inflammation in mice (Mashukova *et al.*, 2009) as well as in inflammatory bowel disease patients by us (Wald *et al.*, 2011) and others (Nakanishi *et al.*, 2018). The next question was whether there is an effect of inflammation-driven aPKC down-regulation in intestinal epithelial cells. Using conditional ablation of PKC ζ/λ in the intestinal epithelium (Prkci^{flox/flox} \times Villin-CRE) in independently derived animal models, we and others showed that loss of function of aPKC in epithelia results in chronic intestinal inflammation (Calcagno *et al.*, 2011; Forteza *et al.*, 2016), mediated by a Th17 response (Nakanishi *et al.*, 2018). Intriguingly, and in apparent contradiction with an extensive body of literature in tissue culture cells and model organisms, the PKC ζ/λ conditional knockout phenotype does not show major loss of epithelial polarity in the intestine (Forteza *et al.*, 2016). Likewise, the double conditional knockout model (Prkci^{flox/flox}, Prkcz^{flox/flox} \times Villin-CRE) shows increased tumorigenesis, but no functional changes in the intestine were reported (Nakanishi *et al.*, 2018). This is puzzling because animal models known to affect apical epithelial polarity such as the Myo5b knockout die of a massive diarrhea within hours after birth (Cartón-García *et al.*, 2015) or show clear transepithelial transport defects related to the defect in polarized membrane proteins such as diarrhea or malabsorption (Xue *et al.*, 2020).

Overall, these results point to the possibility that aPKC in intestinal epithelial cells plays substantial anti-inflammatory roles. The molecular mechanisms regulating innate immunity downstream of aPKC, however, remain unclear. We showed that the Prkci conditional knockout mice display increased NF- κ B activity mediated by the loss of aPKC-mediated phosphorylation of ROCK and nuclear translocation of RelA (Forteza *et al.*, 2016). In culture, this mechanism is cell autonomous (Forteza *et al.*, 2013). However, in vivo, it is enhanced by the intestinal microbiome (Nakanishi *et al.*, 2018). Considering the proinflammatory effects of MARK2 ablation (Hurov *et al.*, 2001; DiBona *et al.*, 2019) and its inhibition by aPKC, we hypothesized that MARK2 may be also involved in innate immunity (NF- κ B) transcriptional effects when up-regulated downstream of aPKC.

NF- κ B proteins such as RelA(p65) and p50 form complexes with I κ B α in the cytoplasm. After NF- κ B proteins translocate to the nucleus, they form different complexes with other transcriptional cofactors such as, for example, the Mediator complex (Nozawa *et al.*, 2017; Soutourina, 2019), Stat1, and Stat2 (reviewed in Platanitis and Decker, 2018) which modulate NF- κ B transcriptional activity, establish cross-talk with other innate immunity pathways, or select subsets of the NF- κ B-activated transcripts. A practical consequence of these interactions is that many partners coimmunoprecipitate with NF- κ B proteins (van Essen *et al.*, 2009). In fact, association of NF- κ B p65 (hereafter referred to as RelA) with Mediator complex proteins, especially with the Med17 (TRAP80) subunit, has been extensively reported (Naar *et al.*, 1999; Park *et al.*, 2003; Owen *et al.*, 2005; van Essen *et al.*, 2009). There is a growing body of evidence indicating that epithelial cells participate in the control of inflammatory processes by secretion of cytokines, beyond their passive barrier function, illustrated by the epithelial-specific IL-10 conditional knockout mice that show intestinal inflammation (Olszak *et al.*, 2014). The interactions between epithelial cell polarity signaling and innate immunity are expected to shed light on the understanding of this underrecognized role of epithelia in organ inflammation.

RESULTS

MARK2 activity increases under TNF α stimulation

Because inflammatory signals posttranslationally down-regulate aPKC in vivo and in culture intestinal epithelial cells (Mashukova *et al.*, 2011; Forteza *et al.*, 2016; Nakanishi *et al.*, 2018), we first analyzed the phosphorylation status of MARK2 in cells stimulated with TNF α . Thr595 is the aPKC phosphorylation target in MARK2 (Suzuki *et al.*, 2004). After confirming PKC ζ down-regulation, we found that, indeed, pT595-MARK2 was consistently decreased in Caco-2 cells stimulated with TNF α while total MARK2 remained unchanged (Figure 1A). Densitometry of three experiments showed a 59% decrease in pT595-MARK2 normalized to total MARK2 (Figure 1B). The decrease in pT595-MARK2 signal was also verified by immunofluorescence (Figure 1C, red signal). Because pT595 is inhibitory for MARK2 activity (Watkins *et al.*, 2008), the loss or decrease of this phosphorylation is expected to increase MARK2 activity.

We verified that MARK2 activity was increased by delocalization of Par3 (Suzuki and Ohno, 2006) in TNF α -stimulated cells. To further test the specific involvement of MARK2, we rescued the effect of TNF α on Par3 by incubating the cells in a specific MARK inhibitor (39621) for the last 4 h of TNF α stimulation. (Supplemental Figure 1A). Also, we wanted to verify that MARK2 is still active under proinflammatory stimulation, as opposed to totally dephosphorylated. We determined that, pT208-MARK, the activation site phosphorylated by STK11(LKB1, serine-threonine kinase 11), was not decreased under TNF α stimulation (Supplemental Figure 1B). In summary, we concluded that TNF α stimulation decreases phosphorylation

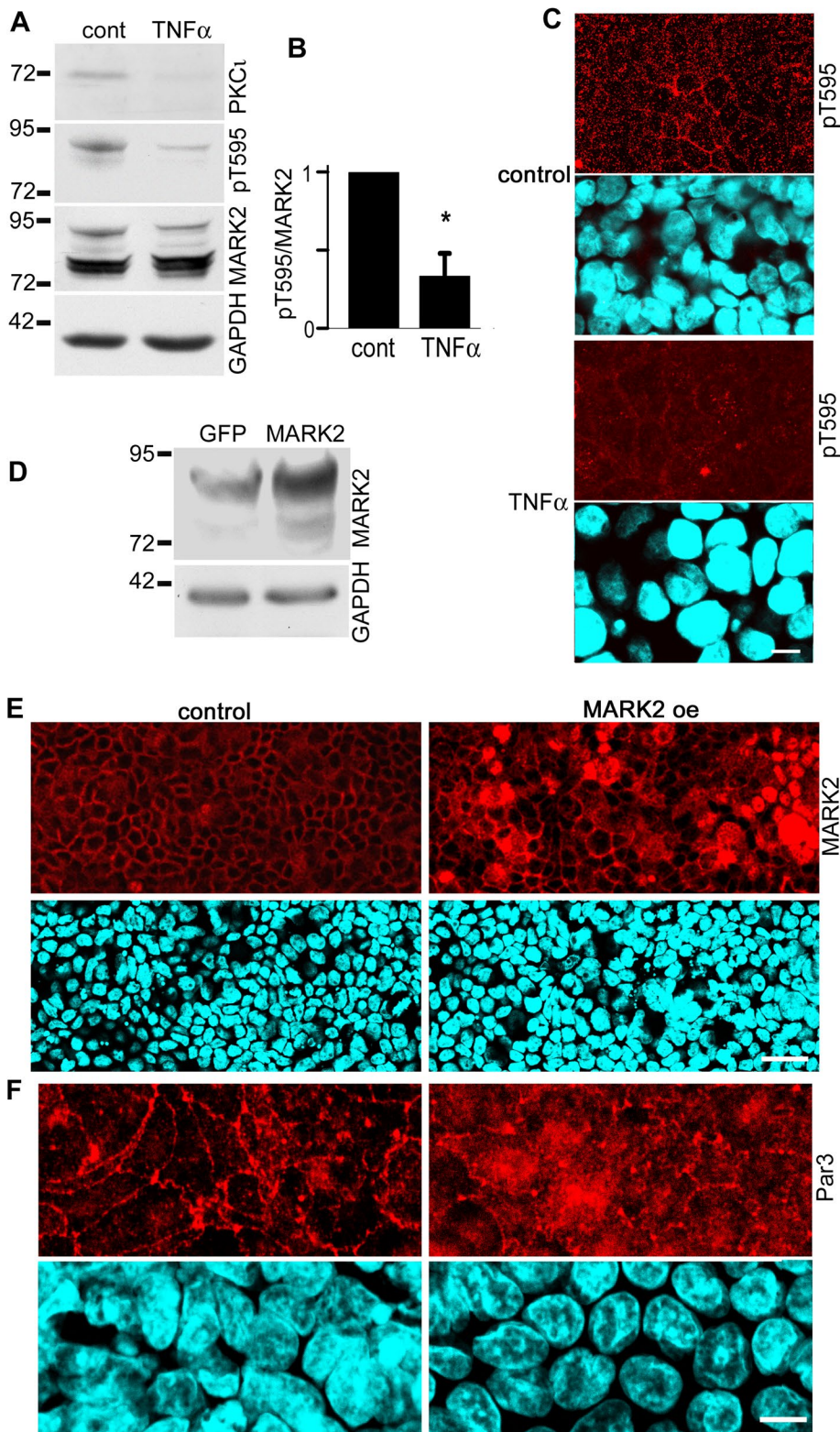


FIGURE 1: Lentivirus-mediated expression of MARK2 mimics innate immunity activation for Par3 distribution. (A) Caco-2 cells grown on filters at confluency for 10 d were stimulated with 20 ng/ml TNF α or vehicle (cont) from the basolateral chamber. Atypical-PKC-mediated phosphorylation of MARK2 in T595 was monitored with a specific antibody. (B) Densitometry analysis of pT595 MARK2/MARK2 in three experiments. * $p < 0.02$. (C) In similar experiments, the cells were analyzed by immunofluorescence with anti-pThr595 MARK2 antibody (red). Bar, 10 μ m. (D) Caco-2 cells were transduced with replication-defective lentiviral particles expressing GFP (control) or MARK2 and selected with puromycin. Cells confluent for 10 d were analyzed by

immunoblot. (E, F) In similar experiments, cells grown on filters were fixed and processed for immunofluorescence using antibodies against (E) MARK2 or (F) anti-Par3. Bars, D, 30 μ m; E, 20 μ m.

in the MARK inhibitory (pT595) site without decreasing phosphorylation in the activation site (pT208), thus up-regulating MARK activity. Then, we hypothesized that overexpression of MARK2 (oe) would mimic increased activity and, thus, the effect of TNF α stimulation. To that end, the cells were transduced with lentiviral particles expressing human MARK2 and selected. As controls we used green fluorescent protein (GFP)-expressing lentivirus or empty vector lentivirus (mock transduction). These negative controls were preferred over kinase-dead MARK2 expression, which has been shown to display increased binding to substrates, thus masking normal interactions of the wt form (Matenia *et al.*, 2012). Increased expression was verified by immunoblot after all transductions (Figure 1D) and by immunofluorescence (Figure 1E). In mock transduced cells, endogenous MARK2 was primarily localized to the lateral membranes. Cells overexpressing MARK2 showed the same lateral membrane distribution of the kinase as in control cells, with additional cytoplasmic localization (Figure 1E). To assess whether the MARK2 overexpression was functional, we verified delocalization of Par3 (Suzuki and Ohno, 2006). As expected, cells overexpressing MARK2 showed Par3 signal broadly distributed in the cytoplasm (Figure 1F). In other words, MARK2 overexpression mimicked the TNF α stimulation effect on Par3, which could be rescued by a specific MARK inhibitor (Supplemental Figure 1A). It is worth noting that TNF α stimulation also delocalized active MARK2 from the basolateral membrane and induced nuclear localization in some cells (Figure 1C; Supplemental Figure 1B, *).

MARK2 overexpression was quantified at the protein level (Figure 2A) and at the mRNA level (Figure 2B) and compared with endogenous MARK2 in control cells transduced with the same lentiviral construct, expressing GFP under the same selection antibiotic. Both determinations showed moderate levels of overexpression, in the 3.5–5-fold range. To test the hypothesis that, like other components of apico-basal polarity signaling, MARK2 modulates NF- κ B transcriptional activity, we used the same GFP- (control) and MARK2-expressing cells

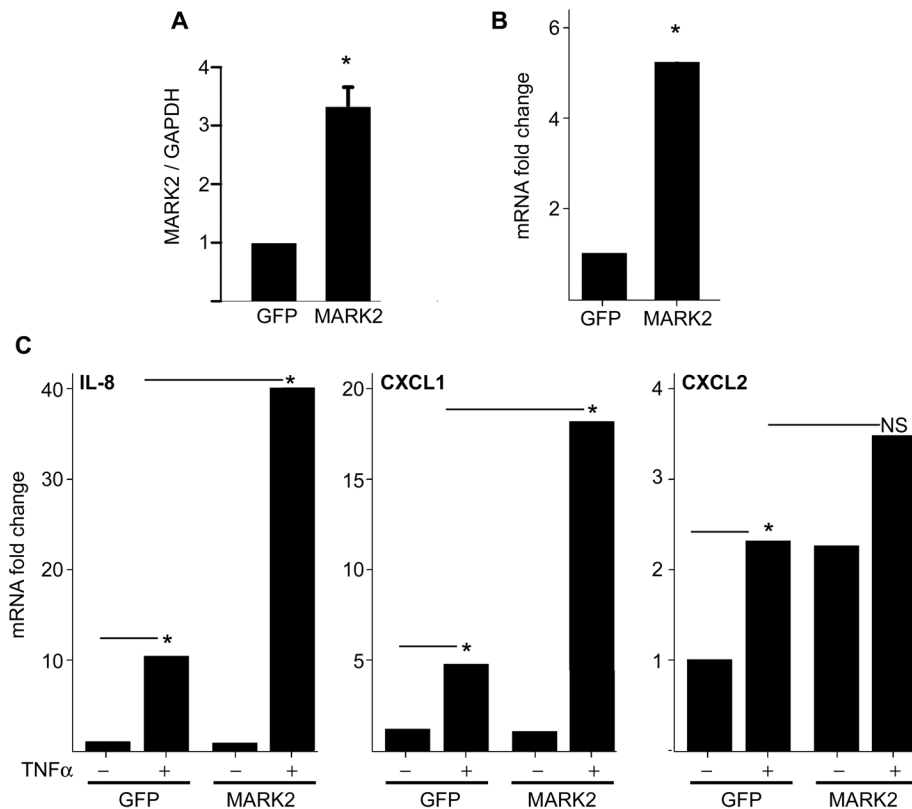


FIGURE 2: MARK2 expression results in enhancement of the NF- κ B transcriptional response of IL-8 and CXCL1, but not CXCL2 to TNF α . (A) Densitometric quantification of MARK2 protein expression in five independent experiments like those shown in Figure 1C, $*p < 0.01$. (B) Fold change in MARK2 mRNA expression determined by RT-qPCR in cells expressing GFP (control) or MARK2. Fold change is not a Gaussian variable; therefore, error bars are not graphed. Significance was calculated using a t test on $\Delta\Delta$ CT values. $N = 4$, $p < 0.01$. (C) Fold change in IL-8, CXCL1, and CXCL2 mRNA expression was determined by RT-qPCR in cells expressing GFP (control) or MARK2. IL-8. Statistical significance was determined using a t test on $\Delta\Delta$ CT values. $n = 7$, $*p < 0.025$; CXCL1, $n = 5$, $p < 0.04$; CXCL2, $n = 5$, NS, not significant.

with and without TNF α stimulation. We determined the expression of three mRNAs regulated by NF- κ B: IL-8(CXCL8), CXCL1, and CXCL2. In control cells, the expression of all three of them significantly increased by TNF α stimulation, a positive control for the assay (Figure 2C). The response to TNF α was significantly enhanced in MARK2-expressing cells for IL-8 and CXCL1 (approximately fourfold over GFP cells stimulated with TNF α), but not for CXCL2 (Figure 2C). These results are consistent with a synergistic effect of MARK2 increased activity on NF- κ B-dependent transcription. Conversely, the lack of response in CXCL2 transcription was puzzling and is analyzed below.

Because transcriptional responses in the NF- κ B pathway require nuclear translocation, we analyzed whether MARK2 overexpression affects RelA subcellular localization. In control (GFP-expressing) cells and MARK2-overexpressing cells RelA remained excluded from the nucleus (Figure 3), which is consistent with lack of transcriptional activation of NF- κ B reporters in the absence of TNF α stimulation (Figure 2C). In addition, these results confirm that the Caco-2 cells naturally display low basal levels of NF- κ B stimulation (Forteza *et al.*, 2013). In contrast, TNF α stimulation resulted in RelA nuclear translocation, which was abolished by an IKK inhibitor (Figure 2A, red channel). The difference between RelA translocation in stimulated control (GFP) and MARK2-expressing cells was not significant (Figure 3, A and B). Altogether, these results suggest that increased

MARK2 activity does not result in changes in NF- κ B nuclear translocation. This is a critical difference with the down-regulation of aPKC, which results in NF- κ B nuclear translocation (Forteza *et al.*, 2016). Likewise, an effective knockdown of MARK2 with two different lentivirus-delivered short hairpin RNAs (shRNAs; termed 81 and 83; Supplemental Figure 2A) did not affect IL-8 mRNA transcription (Supplemental Figure 2B). These data further support the notion that MARK2 increased activity wields transcriptional effects downstream of canonical NF- κ B activation, but is not directly involved in NF- κ B regulation.

MARK2 phosphorylates Ser152-Med17 in complexes with RelA(p65)

To study the molecular mechanism of action of activated MARK2, we considered the possibility that MARK2 may directly associate with NF- κ B complexes and phosphorylate one or more of the NF- κ B proteins or proteins associated with the complex. To test this idea, extracts from GFP- or MARK2-expressing cells were immunoprecipitated with anti-RelA antibodies. We found that MARK2 coimmunoprecipitates with NF- κ B complexes only in MARK2-overexpressing cells (Figure 4A, second to last lane). Because MARK2 target phosphorylation sites generate 14-3-3 binding sites (Lin *et al.*, 2009; Johnson *et al.*, 2010), we analyzed the same immunoprecipitates with an anti-pan 14-3-3 antibody. Consistent with MARK2-dependent phosphorylations in the NF- κ B protein complexes, we found 14-3-3

coimmunoprecipitation with RelA only in MARK2-overexpressing cells (Figure 4A, IP, RelA, second to last lane). If MARK2 and 14-3-3 proteins become physically associated with NF- κ B protein complexes, we reasoned that some proteins in the complex should be phosphorylated. To test this idea, we immunoprecipitated cell extracts from cells expressing GFP (control) or MARK2 with NF- κ B RelA antibody. The immunoprecipitates were then blotted and incubated with recombinant His-tagged 14-3-3 proteins (a mixture of equal amounts of the α , β , δ , ζ , ϵ , η isoforms). Then, the membranes were developed with an anti-His tag antibody in a far-Western blot. Only one band of approximately Mr 80,000 was identified in the NF- κ B complexes as a 14-3-3 partner in MARK2-expressing cells (Figure 4B). A search of all proteins coimmunoprecipitating with RelA revealed that the only known partners of NF- κ B protein complexes in that Mr range are components of the Mediator complex, Med15, Med17, and Med25 (Owen *et al.*, 2005). Of these proteins only Med17 (TRAP80, CRSP6, CRSP77, DRIP80, SRB4, NP_004259.3) showed much higher scores in the proteomic analysis in two different cell lines (Owen *et al.*, 2005). Accordingly, we tested the possibility that Med17 was associated with RelA in our system. In the same blots, we found that Med17 coimmunoprecipitates with RelA in extracts from both MARK2- and GFP-expressing cells (Figure 4B). Then, we asked whether Med17 is directly phosphorylated by MARK2. Cell extracts from nontransduced cells were immunoprecipitated with RelA antibody. After the washes, the

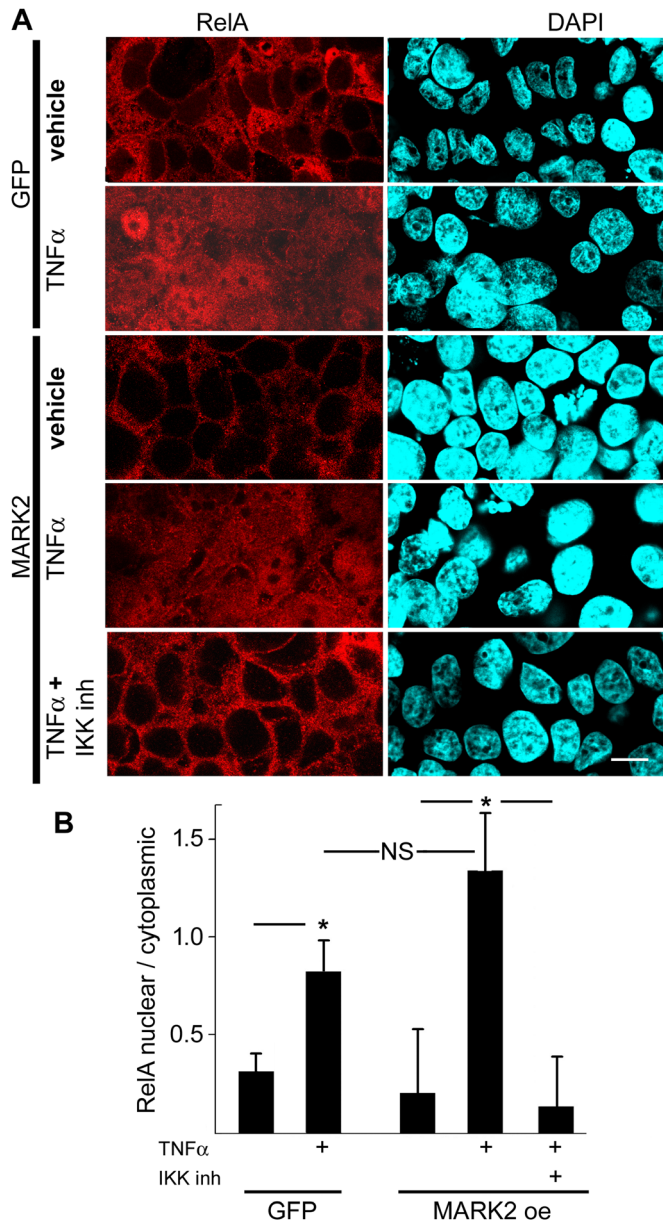


FIGURE 3: RelA-p65 nuclear translocation and MARK2 expression and nuclear localization are independent. (A) Localization of RelA-p65 (red) and DAPI (blue) changes in Caco-2 cells expressing GFP or MARK2 was determined by confocal microscopy in cells stimulated overnight (+) or not (-) with TNF α from the basolateral side. Some of the MARK2-expressing TNF α -stimulated cells were treated with 0.5 μ M PS1145 (IKK inhibitor) along with TNF α . GFP expression marked the control cells. Bar, 20 μ m. (B) Ratios of RelA fluorescence pixel value were calculated in pairs of regions of interest in cell and cytoplasm for each cell. These regions of interest were localized on nucleus or cytoplasm using the DAPI channel, blinded from the RelA signal channel. Averages in nucleus and cytoplasm are shown for GFP-expressing cells (control, 35 cells); GFP+TNF α (33 cells); MARK2-expressing cells (54 cells); MARK2+TNF α (58 cells); and MARK2+TNF α +IKK inh (35 cells) in images from three independent experiments. For graphical purposes, SDs are shown. A Kruskal-Wallis test was performed to determine significance. * $p < 0.005$; NS, not significant.

immunoprecipitates still attached to the beads were incubated in the presence or absence of ATP with purified, recombinant, active MARK2. Supernatants (SN) and bead eluates (pellet) were blotted.

To identify MARK2 phosphorylation targets the blots were overlaid with His-tagged 14-3-3 proteins and analyzed by far-Western blot as in Figure 4B. Consistent with the experiments in Figure 4B, only one 80,000 band binding to 14-3-3 in a far-Western blot coimmunoprecipitated with RelA under phosphorylation conditions (MARK2+ATP, Figure 4C). In parallel blots, we found that under non-phosphorylation conditions (-ATP) Med17 was fully associated to the immunoprecipitate (pellet) (Figure 4C). Therefore, the 80,000 Mr band is directly phosphorylated by MARK2 in vitro.

To further corroborate that Med17 is a phosphorylation target of MARK2, we conducted in vitro phosphorylation of recombinant Med17 with MARK2 in the presence or absence of ATP and analyzed the results by mass spectrometry. Only the Ser152-Med17 site was found differentially phosphorylated (Figure 4D). This was unexpected because it is not the potential 14-3-3 site predicted with the highest score (<http://www.compbio.dundee.ac.uk/1433pred>) in Med17 and lacks the Gly residue in the MARK2 consensus sequence (KXGS [Drewes et al., 1997]). On the basis of the mass spectrometry data, we decided to validate the Ser152 phosphorylation site by expressing HA-tagged S152A- and S152D-Med17 mutants, along with the wild-type (wt) form. The mutants were expressed using lentiviral vectors and antibiotic selection. All three of them were found at the 80,000 Mr range by HA-tag blot and were expressed at similar levels (Figure 4E). It must be noted that the cells expressing S152D-Med17 reached confluency at a slower pace and had to be seeded at higher densities to synchronize them with the other cultures for confluence. All the experiments that follow were performed under similar confluency conditions for the two mutants and the wt protein. Even though these cell lines were stable transductions, the S152D cells lost their Med17 mutant expression within a few passages. Accordingly, all the experiments reported below used cells within the first five passages after lentiviral transduction. Wt HA-Med17 and the S152A-Med17 mutant coimmunoprecipitated with RelA (Figure 4E) mimicking nonphosphorylated endogenous protein (Figure 4C).

We analyzed the subcellular distribution of HA-tagged wt Med17 and Ser152 mutants to make sure that they display nuclear localization, a necessary condition to exert transcriptional regulation. By HA signal immunofluorescence, we found that most cells in the culture expressed similar levels of HA signal at few passages (<5) after transduction (Figure 5). Both mutants and the wt protein showed nuclear localization as expected. The S152A mutant, however, showed also cytoplasmic distribution in stark contrast with the phosphomimetic mutant which was strictly nuclear (Figure 5A). This is consistent with coimmunoprecipitation of the nonphosphorylated Med17 with RelA (Figure 4) possibly in cytoplasmic complexes. Conversely, the phosphomimetic mutant was only nuclear, suggesting that it may form complexes with transcriptional regulators (Figure 5A). Endogenous Med17 was concentrated in nuclei but also present in the cytoplasm (Figure 5B).

Expression of Med17 and S152D-Med17 mimic MARK2 overexpression effects on NF- κ B-regulated transcription

To establish the functional role of Med17 S152 phosphorylation, we wanted to determine whether expression of wt Med17 and the Ser152 mutants mimic MARK2 overexpression at the level of transcriptional regulation of NF- κ B-dependent transcripts. To that end, two transcripts regulated by the Mediator complex (Chen et al., 2017), IL-8 and CXCL1, and one Med17-independent transcript, CXCL2 (van Essen et al., 2009) were assayed under two experimental conditions: 1) coexpression with MARK2 and 2) external stimulation with TNF α . Expression of wt Med17, S152A, or S152D mutants alone

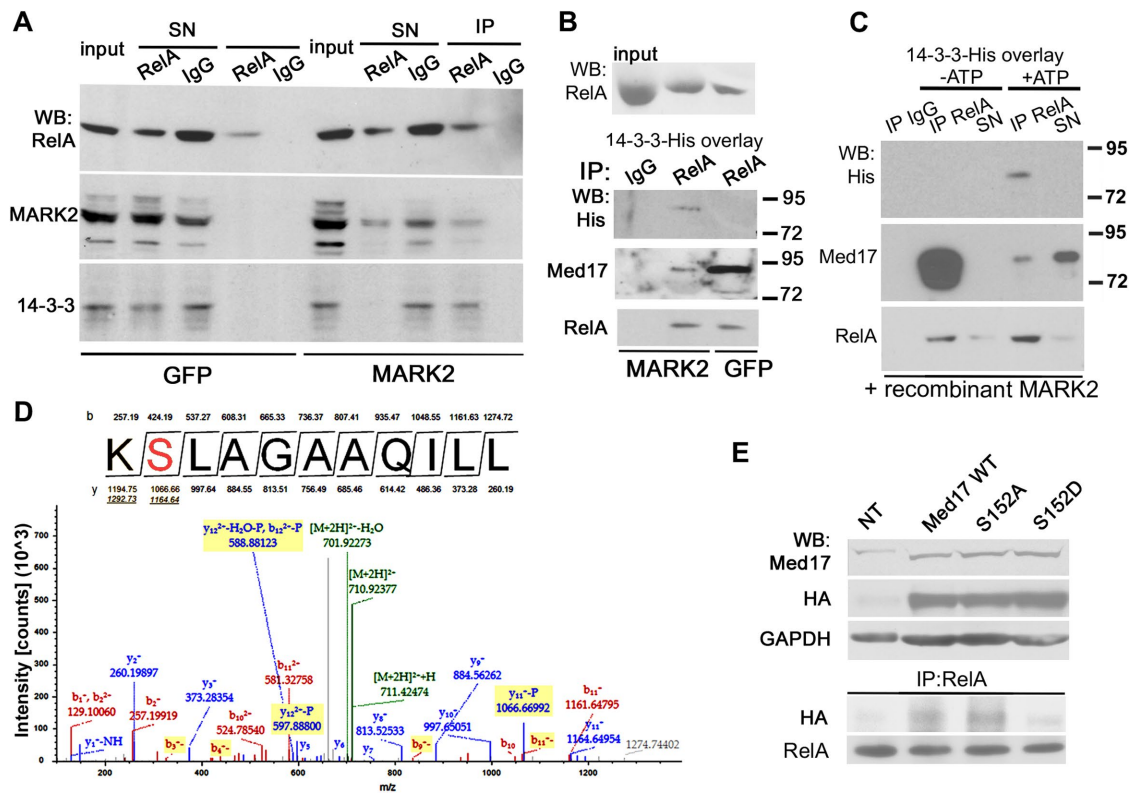


FIGURE 4: MARK2 phosphorylates core Mediator component Med17 in NF- κ B complexes. (A) MARK2 and 14-3-3 coimmunoprecipitated with RelA in extracts from Caco-2 cells overexpressing MARK2 but not in controls expressing GFP. Nonimmune rabbit IgG was used as a negative control for immunoprecipitation. The supernatant after immunoprecipitation (SN) and the eluate from beads (IP) were analyzed by immunoblot. (B) In similar experiments, immunoprecipitates from GFP- or MARK2- expressing cells were blotted and overlaid with His-tagged recombinant 14-3-3 proteins (α , β , δ , ζ , ϵ , η). The blots were then analyzed by anti-His tag antibody in “far-Western” mode. Parallel blots were analyzed with anti-Med17 and RelA antibodies. (C) Nontransduced cell extracts were immunoprecipitated with anti-RelA antibodies (or IgG) and exposed to recombinant active MARK2 in the presence or absence of 1 mM ATP before eluting the protein G beads. After incubation, the supernatant (SN) and the eluates of the beads (pellet) were electrophoresed and blotted. The blots were overlaid with His-tagged recombinant 14-3-3 proteins and then developed with anti-His tag antibody (far-Western blot) as in B. Parallel blots of in vitro phosphorylated RelA immunoprecipitates were immunoblotted with anti-Med17 antibody. Localization of Mr standards is $\times 10^3$. (D) Mass spectrometry profile of pSer152, which was the only Med17 site phosphorylated by recombinant MARK2 detected. Result is representative of three experiments. (E) Cells transduced with lentiviral particles and selected express similar amounts of HA-tagged wt Med17 and S152A and S152D mutants, NT, nontransduced Caco-2 cells. Cell extracts from these stable cell lines were immunoprecipitated with RelA and immunoblotted with anti-HA or RelA antibodies

had no significant effect on the expression of any of the three reporter mRNAs. Coexpression of wt Med17 and MARK2 resulted in a significant fivefold increase for IL-8 mRNA, but not CXCL1 or CXCL2, which was abolished in cells expressing the nonphosphorylatable Med17 mutant (Figure 6). In the presence of TNF α , however, expression of wt Med17 resulted in a significant twofold increase in IL-8 mRNA over the level of TNF α -stimulated GFP-expressing Caco-2 cells (Figure 6). This result mimics the synergy of MARK2 expression with canonical NF- κ B stimulation (Figure 2). As in the case of MARK2 expression, this phenomenon was not observed for CXCL2 mRNA expression. The levels of IL-8 and CXCL1 mRNA expression under TNF α stimulation in the presence of S152A Med17 were indistinguishable from the expression in stimulated GFP Caco-2 cells and significantly lower than in cells expressing the phosphomimetic mutant. That is, the synergy between Med17 expression and TNF α stimulation was abolished by the nonphosphorylatable mutant.

These results are consistent with a role of Med17 S152 phosphorylation in the regulation of NF- κ B transcriptional function downstream of canonical activation of NF- κ B. In other words,

pSer152-Med17 enhances transcription of IL-8 and CXCL1 after NF- κ B has translocated to the nucleus. Conversely, the lack of response of CXCL2 mRNA transcription enhancement with both MARK2 overexpression (Figure 2) and Med17 (Figure 6) may be explained by the fact that CXCL2 belongs to a category of NF- κ B-regulated transcripts that is independent of Med17 (van Essen et al., 2009).

Atypical PKC λ /i knockout induces changes in Med17-dependent transcripts in vivo

Previous data suggest a model in which increased MARK2 activity arising from proinflammatory signals results in phosphorylation of S152-Med17. These results were observed on targeted transcripts dependent of Med17 and NF- κ B. To test the predictions of this model in vivo, we used a tissue-specific (villin-CRE) Prkci^{flox/flox} knockout model that lacks aPKC in the intestinal villus epithelium (Forteza et al., 2016). This is because the other aPKC isoform, PKC ζ , is not expressed in villi. These mice develop spontaneous chronic intestinal inflammation via NF- κ B (Forteza et al., 2016) enhanced by the microbiome (Nakanishi et al., 2018).

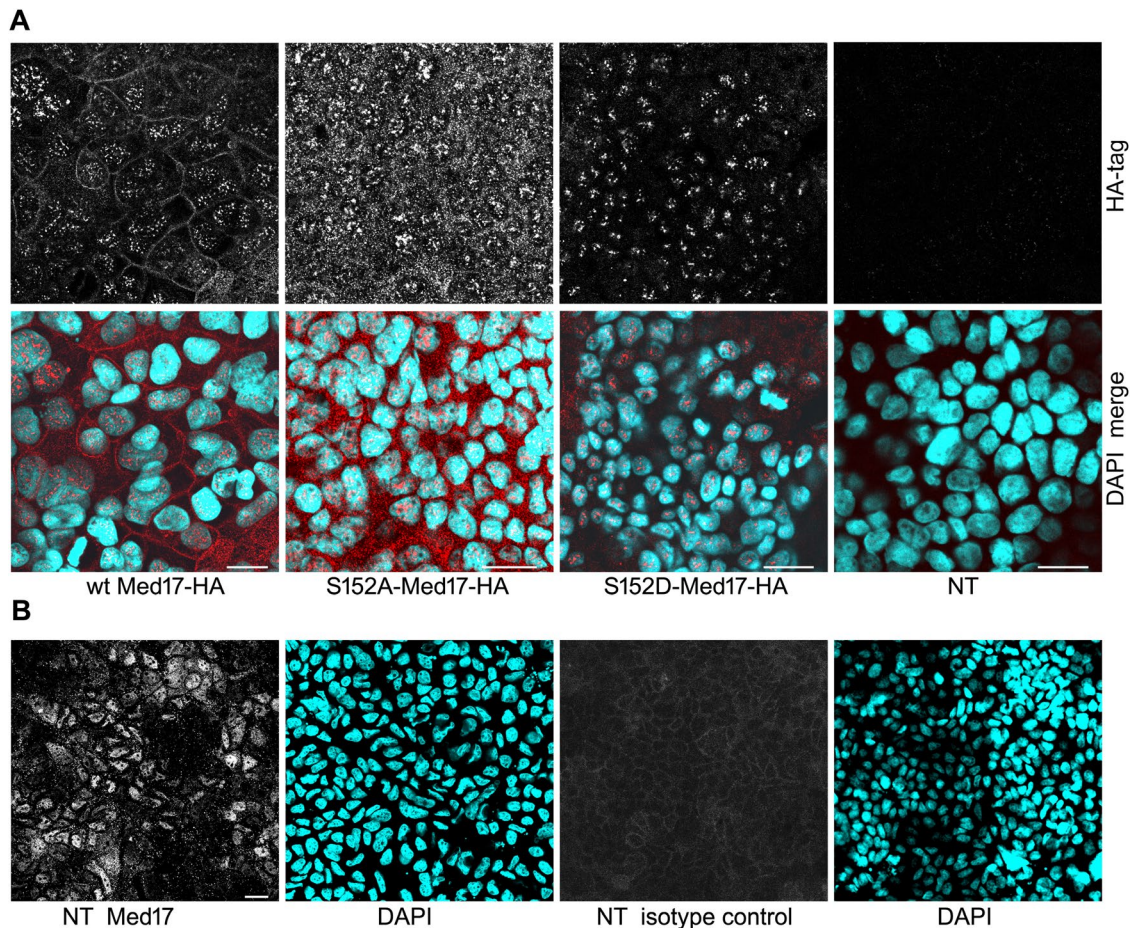


FIGURE 5: Ser152-Med17 mutants display differences in cytoplasmic localization. (A) Caco-2 cells were transduced with HA-tagged wt-, S152A-, and S152D-Med17 or nontransduced (NT). Low-passage cultures (fewer than five passages after transduction) were grown on filters at confluency for 10 d, fixed, and processed with anti-HA tag antibody (top panels; red in bottom panels) and DAPI. (B) Nontransduced cells were processed with either anti-Med17 antibody or isotype control. Scale bars, 20 μ m.

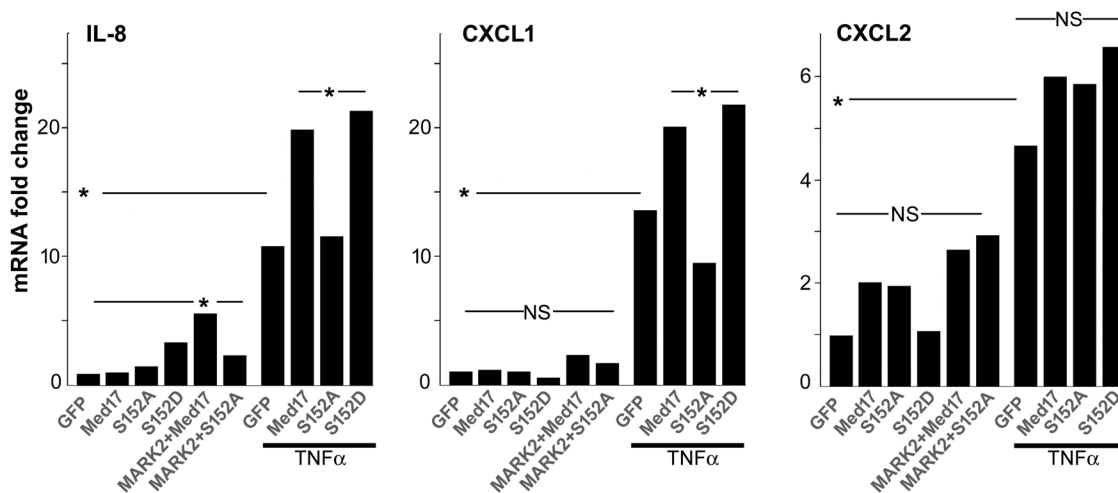


FIGURE 6: Med17 modulation of NF- κ B signaling is regulated by Ser152-Med17 mutants. Caco-2 cells were transduced with lentivirus expressing wild-type Med17 (wt), S152A-Med17, S152DMed17, or GFP(control) and selected. Some cells were double-transduced with MARK2 and wt Med17 or S152D-Med17, under double selection. GFP-expressing cells and cells expressing wt Med17 and the S152 mutants were also stimulated with 20 ng/ml TNF α . Expression of IL-8, CXCL1, and CXCL2 mRNAs was analyzed by qPCR. For graphical purposes fold change ($2^{\Delta\Delta Ct}$) as compared with GFP nonstimulated Caco-2 cells is shown as average. SDs are not shown because fold change is not Gaussian. For statistical significance, a t test (comparisons between pairs of data) or analysis of variance for multiple treatments was applied on $\Delta\Delta Ct$ values. * $p < 0.03$, $n = 7$.

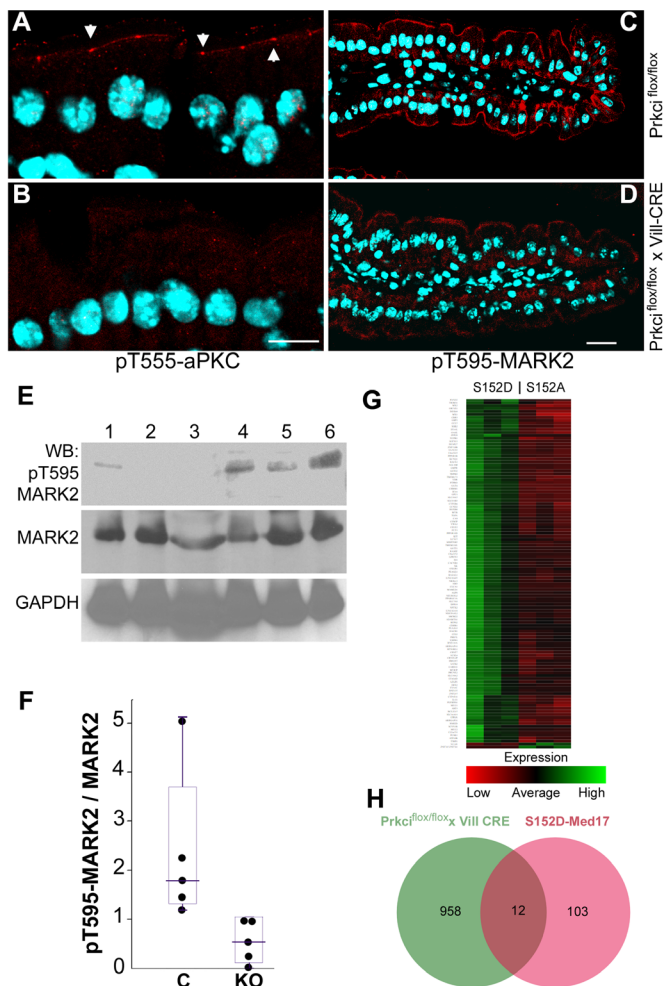


FIGURE 7: PKC λ knockout mice show pT595-MARK2 down-regulation and changes in the Med17-dependent transcriptome. (A) Prkci^{fllox/fllox} duodenal villus epithelial cells (as a control for KO) were stained with anti-aPKC pT555 antibody. Arrows show apical localization of aPKC(i/l and z). (B) Prkci^{fllox/fllox} x Vill-CRE villus cells were stained with the same antibody. Bar, 10 μ m. Duodenal villi of (C) Prkci^{fllox/fllox} and (D) Prkci^{fllox/fllox} x Vill-CRE jejunum sections were stained with anti-MARK2 pT595 antibody. Villi are shown. Bar, 20 μ m. (E) Extracts of duodenal mucosae from Prkci^{fllox/fllox} x Vill-CRE (lanes 1–3, KO) and Prkci^{fllox/fllox} (lanes 4–6, control) mice were probed by immunoblot. (F) Densitometric analysis of the ratios of signals pT595-MARK2/MARK2 were normalized to the highest value in the control group. Box-and-whisker plot is shown. Both groups were statistically different, Kruskal–Wallis test $p < 0.001$ ($n = 5$). (G) RNAseq heatmap generated from gene expression induced by transduction with S152D-Med17 as compared with S152A-Med17-expressing cells in the presence of 10 ng/ml TNF α ($n = 3$ pairs, $p < 0.03$, counts > 10). CXCL1 and –8 transcripts appeared below 10 counts each and were not included. (H) Venn diagrams of the set of transcripts described in G (pink), and transcripts showing significant changes of mRNA expression in Prkci^{fllox/fllox} x Vill-CRE jejunum mucosae as compared with Prkci^{fllox/fllox} ($n = 3$ pairs, $p < 0.005$) (green).

As shown before (Forteza et al., 2016), aPKC in the active conformation (pT555-aPKC) signal was restricted to the vicinity of tight junctions in villus enterocytes in control animals (Figure 7A, arrows) but absent altogether in Prkci^{fllox/fllox} x Vill-CRE (KO) cells (Figure 7B). Because the sequence around this phospho site is identical in PKC ζ and ι/λ , the antibody reports on both isoforms of aPKC. In parallel

sections, shown at lower magnification, we stained for pT595-MARK2. As expected, the signal was decreased in the aPKC-deficient villus cells (Figure 7, C vs. D). The same result was verified by immunoblot of duodenal mucosal extracts (Figure 7E). Comparative densitometry of blots from Prkci^{fllox/fllox} (c) or Prkci^{fllox/fllox} x Vill-CRE normalizing pT595-MARK2 signal to total MARK2 signal showed a significant fourfold decrease in Thr595-MARK2 phosphorylation in the knockout mice (Figure 7F).

We conclude that in aPKC-deficient enterocytes, MARK2 is functionally up-regulated by a decrease in pT595 phosphorylation, which changes to a similar extent as in Caco-2 cells stimulated with TNF α (Figure 1B).

Functional implications of changes in the transcriptome induced by Prkci deficiency in mouse enterocytes and S152D-Med17 mutant expression in Caco-2 cells

To identify the range of the effects of Ser152-Med17 phosphorylation, we transduced Caco-2 cells with S152D-Med17 or S153A-Med17 and compared the transcriptomes under TNF α stimulation. We found 115 transcripts significantly changed, in most cases up-regulated. Only two transcripts were down-regulated (VCAN, a chondroitin sulfate proteoglycan; and ZNF765-ZNF761, a transcriptional regulator) (Figure 7, G and H, pink). A similar study was conducted comparing mRNA extracts from duodenal mucosae of Prkci^{fllox/fllox} x Vill-CRE conditional knockout mice with Prkci^{fllox/fllox} controls. In this case, we found 970 transcripts significantly up-regulated (Figure 7H, green). Importantly, we verified that at least 12 of the transcripts up-regulated in the Prkci conditional knockout mucosae were up-regulated by expression of S152D-Med17 (Figure 7H). Of these, eight are directly involved in innate immunity responses (Table 1, bold lettering). Moreover, three genes that control interferon pathways (DDX60, IFI44L, TMEM173/STING) were found in this set of genes. Five genes were identified in transcription control databases as induced by NF- κ B and one by the IFN signaling (Table 1). Because these experiments were conducted on TNF α -stimulated cells, the NF- κ B-dependent genes were synergistically up-regulated by S152D-Med17 above the maximum expression due to NF- κ B. Unfortunately, CXCL8 and CXCL1 transcripts identified with quantitative polymerase chain reaction (qPCR) were below the detection sensitivity of RNAseq. However, they have been reported by other groups (Sturm et al., 2005) in the same cells, so we conclude that at least seven transcripts are synergistically up-regulated by pSer152-Med17.

To better understand the biological implications of the PKC λ knockout and the S152D-Med17 phosphorylation, we analyzed the gene ontology (GO) of both sets of transcripts. PKC λ -deficient enterocytes, as expected, showed significant enrichment in transcripts related to several functions of innate immunity, cytokine expression, and response to bacteria (Supplemental Table 2). The S152D-Med17-induced transcripts, however, showed significant enrichment only for antiviral responses ($p = 4 \times 10^{-6}$, $q = 3.2 \times 10^{-2}$; Supplemental Table 2). We conclude that the MARK2–Med17 axis controls a specific subset of genes regulated during the innate immunity response in epithelial cells. Not surprisingly, other unrelated gene transcripts were also up-regulated by Med17 expression. Their functional significance remains to be determined.

DISCUSSION

In this work, we analyzed the hypothesis that a mild increase in MARK2 activity resulting from aPKC down-regulation or proinflammatory signaling is involved in the control of innate immunity pathways. We found that, indeed, there is a decrease in pThr595-MARK2

Gene	Function	TR
CBR3	Inflammation-induced antioxidant	NF-kB
CEMIP	Inflammation-induced hyaluronidase	Nf-kB
DDX60	Antiviral factor, promotes RIG-I activity	IRFs
GPRIN3	Gai/o protein signaling	
HOXB8	Homeobox transcription factor	
IFI44L	Interferon regulatory factor	
KIT	Signaling, involved in interleukin signals	
PCSK1	Protein convertase	NF-kB
SGK2	Serum/glucocorticoid-regulated kinase-2	
SLC5A8	Apical solute transporter	
TMEM173	STING. Sensor of cytosolic DNA. Regulation of interferon pathway	NF-kB
CCL5	RANTES, small chemokine	NF-kB

Bold lettering, genes involved in innate immunity; TR, transcriptional regulation, obtained through TRRUST search page (gnpedia.org) and http://fiserlab.org/tf2dna_db/search_genes.html, refers to genes that include NF-kB or IRFs (IFN pathway) among other transcriptional regulators.

TABLE 1: Common elements in S152D-Med17- and *Prkci*^{fllox/fllox} x Vill-CRE-induced transcripts.

in cultured intestinal cells under TNF α stimulation, as well as in PKC ζ / λ -deficient enterocytes in vivo. A fourfold overexpression of MARK2 did not modify NF-kB nuclear translocation or result in increased NF-kB transcriptional activity per se, but significantly enhanced the transcriptional response to NF-kB canonical activation of two out of three NF-kB-dependent cytokines. While we have not directly tested TLR4, it is reasonable to speculate that it may exert the same type of stimulation in vivo as TNFR does in culture, because they share the same downstream effects on canonical NF-kB stimulation (Yang *et al.*, 2020). Therefore, the experimental use of TNF α as an activator of the canonical NF-kB pathway in this work seems commensurate with the in vivo effect of the microbiome. CXCL2, a cytokine gene that does not require Med17 for transcription, was the exception. The major difference of PKC ζ / λ knockout with MARK2 overexpression is that the former activates NF-kB nuclear translocation via ROCK and, accordingly, also induces CXCL2 transcription, even in the absence of TNF α signaling (Forteza *et al.*, 2016). Thus, the data suggest two parallel, possibly synergistic pathways downstream of aPKC loss of function: one mediated by ROCK acting on the canonical NF-kB activation reported before (Forteza *et al.*, 2016), and the other described here, which is mediated by MARK2 acting via Med17 on a subset of NF-kB-dependent transcripts. The two-parallel-pathways model was supported by transcriptome analysis. Not only was the number of transcripts up-regulated in aPKC-deficient intestinal epithelia roughly ninefold the number up-regulated by Med17 overexpression, the enrichment in subsets of transcripts with a defined ontology was also different.

The phenotype of MARK2 overexpression described here is also like that of Par3 knockdown described before, which could be rescued by expression of active PKC ζ (Forteza *et al.*, 2013). The only difference between Par3 knockdown and MARK2 overexpression is that the former resulted in RelA nuclear translocation. We speculate that Par3 knockdown may have acted through aPKC, thus activating the two parallel pathways, while MARK2 overexpression is downstream of aPKC.

We first identified a MARK2 target by 14-3-3 coimmunoprecipitation with NF-kB RelA protein complexes. However, the Med17 interaction with NF-kB is possibly one among several effects downstream of aPKC, as indicated by transcriptomics data. It is worth noticing that the RNAseq studies have two confounding factors: 1)

The mRNAs isolated from mouse mucosae did show some contamination with underlying mesenchymal cells. Because aPKC deficiency in enterocytes is known to result in macrophage recruitment to the lamina propria (Nakanishi *et al.*, 2018), the overall changes in the transcriptome may include mRNAs from immune cells. Accordingly, the transcripts also expressed in Caco-2 cells provide a good sampling of the cell-autonomous effects in the epithelium. 2) The expression levels of some critical mRNAs in Caco-2 cells were very low. That was the case of CXCL1 and CXCL2. Both transcripts showed fewer than 10 counts and could not be used for the RNAseq analyses. This is despite expression of both transcripts and the corresponding proteins has been documented in Caco-2 cells for many years (Yang *et al.*, 1997). In fact, we could easily detect CXCL transcripts by qPCR. This sensitivity caveat leaves open a possibility that there may be more transcripts regulated by 152Ser-Med17 phosphorylation that were not detected in this study. Even bearing that in mind, we conclude that MARK2 up-regulation-Med17 phosphorylation is a novel signaling pathway conveying information from the cell surface directly to transcriptional regulation. Some of the transcripts are under NF-kB activation, and the Med17 effect is synergistic with innate immunity signals. For example, IL-8/CXCL8, CXCL1, and Rantes (Table 1) are all chemoattractants for macrophages. Additional studies may be necessary to determine the physiological role of the transcripts up-regulated by pSer152-Med17, which are not dependent on aPKC. It is conceivable that other kinases may phosphorylate the same site under different conditions. Some of these transcripts may be important in the multiple pleiotropic effects of MARK2, which exceed the focus of this study.

A large body of published evidence in epithelial cell polarity interprets the results of Par (partition defective) protein manipulations as cytoplasmic, "local" to the cell cortex. However, the field has largely not explored hypotheses involving innate immunity effects of polarity signaling or additional transcriptional effects downstream of aPKC or MARK2. For example, the Par1b/MARK2-deficient *C. elegans* embryos were arrested in their development and formed amorphous cellular masses (Kemphues *et al.*, 1988), a phenotype that could be interpreted as not depending exclusively on cell polarity defects. In addition, it was surprising to find that 152Ser-Med17 phosphorylation up-regulates an apical membrane transporter transcript (SLC5A8), a finding validated in aPKC-deficient

mice (Table 1). Therefore, the results here add evidence suggesting that some of the effects resulting from experimental manipulation of molecules traditionally thought to regulate cell polarity may also result from broader changes in the transcriptome, including, but not restricted to, innate immunity regulation.

MATERIALS AND METHODS

Request a protocol through *Bio-protocol*.

Reagents

Recombinant human TNF α , with carrier, was obtained from R&D Systems (cat# 210-TA). It was aliquoted and stored at -70°C . The IKK inhibitor PS1145 dihydrochloride (Yemelyanov *et al.*, 2006; Lung *et al.*, 2019) was obtained from Tocris (cat# 4569). It was stored as a stock solution in dimethyl sulfoxide (DMSO) (50 mM) and used at a final concentration of 0.5 μM . This concentration is well above the IC50 for IKK inhibition but below the IC50 for other effects and inhibition of known kinases (Lam *et al.*, 2005). MARK/Par1 inhibitor 39621 was purchased from EMD Millipore (cat# 454870). It was also stored as a DMSO stock solution (20 mM) and used at final concentration of 10 μM . That is approximately fourfold the IC50 for MARK kinases and 0.4-fold the known IC50 for other kinases (Timm *et al.*, 2011). Halt Protease Inhibitor Cocktail (cat# 78430) and Halt Phosphatase Inhibitor Cocktail (cat# 78420) were obtained from Thermo Fisher Scientific (Waltham, MA) and used at manufacturer-recommended final dilutions. Pierce ECL Western Blotting Substrate was also from Thermo Fisher Scientific (cat# 32209).

Constructs and lentiviral particles

Artificial genes of HA-tagged wt Med17 and Ser152 Med17 mutants were prepared by Genscript and checked by full forward and reverse sequencing and provided in a pEZ-Lv151 vector. The constructs were recloned into lentiviral vectors.

OmicsLink Expression-Ready ORF cDNA Clones expressing eGFP or Par1b(MARK2) in the LV-105 backbone vector (CMV promoter, puromycin stable selection) were obtained from GeneCopoeia (Rockville, MD). All lentiviral vectors were packaged into non-replicating lentiviral particles using the Lenti-Pac HIV Expression Packaging kit from the same supplier.

Antibodies

Antibodies, sources, and validation are detailed in Supplemental Table 1. Secondary antibodies were affinity purified and obtained from Jackson ImmunoResearch Laboratories, West Grove, PA.

Recombinant proteins

Recombinant human His-tagged 14-3-3 proteins (α , β , δ , ζ , ϵ , η) were purchased from GeneCopoeia. MARK2 Recombinant Human Protein (PV3878) expressed by baculoviral vectors was obtained from Invitrogen Life Technologies. Med17 (TRAP80) Recombinant Human Protein (H00009440) was obtained from Novus Biologicals.

Cells, transduction, and selection

Caco-2 (human adenocarcinoma) cells were obtained from and validated by the American Type Culture Collection (ATCC) once a year. These cells are contact inhibited and differentiate in polarized monolayers, especially when grown on filters. After 10 d of confluent culture on Transwell filters (Corning), they express membrane transporters and enzymes typical of human villus enterocytes, tight junctions, and desmosomes, brush border, as well as a fully established apico-basal polarity. Accordingly, the cells display electrophysiological properties like those of intestinal epithelia (Grasset

et al., 1984) and a transcriptome closely related to human enterocytes (Tremblay *et al.*, 2006). Caco-2 cells were maintained and grown as described before. For experiments, the cells were grown on Transwell filters. Transduction and selection were performed as described before (Mashukova *et al.*, 2009). In brief, to package the virus, HEK293T cells were cotransfected using a replication-defective lentiviral vector and packaging plasmid using the manufacturer's recommendation (GeneCopoeia; cat# Clv-PK-01). Subsequently, sparse Caco-2 cells, 24 h after seeding on plastic dishes, were infected with lentiviral particles for 24 h and selected with appropriate antibiotics (0.5 $\mu\text{g}/\text{ml}$ puromycin and/or 500 $\mu\text{g}/\text{ml}$ geneticin G418 Sulfate (Invitrogen, Carlsbad, CA) until dead/detaching cells were no longer observed (typically after 5–7 d). Following growth to confluency, cells were trypsinized and replated onto filter inserts for experiments or plastic dishes for stock. Stock cultures were kept continuously under antibiotic selection. The expression of transduced protein or the knockdown effect of shRNAs was monitored by immunoblot in each passage. Typically, the cells were used for up to 5–10 passages after transduction, except for Med17 mutant-expressing lines, which were used within five passages from the lentiviral transduction. All the experiments reported here were repeated in cells from at least three independent transductions.

Immunofluorescence and image quantification

Immunofluorescence was performed after fixation in 4% formaldehyde, freshly prepared from paraformaldehyde, and permeabilization in 0.4% Triton X-100 in phosphate-buffered saline (PBS). For detection of phosphorylated epitopes, fixation was in 5% trichloroacetic acid (TCA) as described before (Hayashi *et al.*, 1999). For immunofluorescence of HA-tagged Med17, the cells were fixed in 95% methanol at -20°C for 30 min. The maximum projections of 10 confocal optical sections at the apical side of the cells were shown for Par3 immunofluorescence, along with 10 confocal sections at the basolateral (nuclear) level from the same stacks for DAPI. Maximum projections were necessary because of the uneven shape of the apical surface in columnar cells grown on filters.

Mouse intestine frozen sections were obtained after fixation of tissue in 5% TCA, infusion in 30% sucrose in 1:10 PBS for 4 h, and freezing in Tissue-Tek optional cutting temperature compound in isopentane at melting point. Like images from cultured cell monolayers, frozen sections were also imaged by confocal microscopy using a Leica TS5 confocal instrument and LAS software for image acquisition. Images were acquired using the Leica 63 \times immersion objective (NA 1.3).

Pixel values were measured as described before (Wald *et al.*, 2011). Briefly, for quantification of RelA nuclear translocation, random regions of interest were located blinded from the RelA signal on nuclei or adjacent cytoplasm using the DAPI channel alone. The ratio of cytoplasm/nuclear signal was then calculated for each cell with 10 or more replicates and in three or more independent experiments. Typically, the ratio was less than 0.5 for nonstimulated cells and more than 0.9 for TNF α -stimulated cells.

RNA isolation and RT-qPCR (real-time polymerase chain reaction)

Total RNA was isolated using Omega Bio-Tek Homogenizer Columns and the E.Z.N.A Total RNA Kit I (Omega Bio-tek, Norcross, GA). One microgram of total RNA was reverse transcribed to cDNA with iScript cDNA Synthesis Kits (Bio-Rad, Hercules, CA). qPCR was performed using the CFX Connect qPCR instrument (Bio-Rad, Hercules, CA), and TaqMan gene expression universal assays were used to measure transcription of human IL-8, CXCL1, CXCL2, MARK2,

and GAPDH obtained from Thermo Fisher Scientific (Waltham, MA). Cycle numbers were normalized to human GAPDH endogenous control. Transcript level fold differences between different samples were calculated by $\Delta\Delta CT$ (ddCT) comparative cycle threshold (Livak and Schmittgen, 2001)

Protein extraction, immunoblot, and blot overlay (far-Western blot)

Protein extraction from tissue culture cells for PAGE was performed in 1% SDS sample buffer, followed by sonication and heating at 95°C. Protein extraction from intestinal mucosa was performed after two washes of the unopened lumen in ice-cold 10 mM EDTA, 5 mM dithiothreitol [DTT] in PBS supplemented with anti-proteases and anti-phosphatases cocktails. After fully draining the intestinal lumen it was filled up with RIPA buffer solution (150 mM NaCl, 1 mM EDTA, 1 mM EGTA (Ethylene glycol-bis(β -aminoethyl ether)-*N,N,N',N'*-tetraacetic acid), 20 mM Tris, pH 8.0, 1% NP-40 [IGEPAL CA-630] and 1% sodium deoxycholate) supplemented with anti-protease and anti-phosphatase cocktails (2 ml for the full length of the intestine) and drained after 1 min. The extracts were sonicated, spun at 15,000 $\times g$ at 4°C for 10 min, aliquoted, and frozen immediately. One of the aliquots was used for protein determination. For PAGE, aliquots were rapidly thawed, and 30 μg of protein/lane was mixed with an excess of SDS sample buffer (typically 1:10 vol/vol).

Immunoprecipitation

At 10 d after seeding cells on a 24 mm Transwell insert, total proteins were extracted from Caco-2 cells expressing either MARK2 or GFP with RIPA buffer. The samples were sonicated and spun at 15,000 $\times g$ for 15 min in the cold. Supernatants were subjected to total protein quantification using the BCA protein assay and preadsorbed with Protein G PLUS-Agarose (Santa Cruz Biotechnology, Dallas, TX). Extracts (50 μg) were immunoprecipitated at 4°C with mouse anti-RelA antibody (0.01 mg/ml final concentration) or mouse nonimmune immunoglobulin G (IgG) for control extracts followed by an incubation with Protein G PLUS. Immunoprecipitates were centrifuged at 2500 rpm for 5 min at 4°C. Following five washes with RIPA solution and one final wash with Tris buffer, pH 6.8, immunoprecipitate samples were eluted in sample buffer before SDS-PAGE analysis.

For in vitro phosphorylation experiments, immunoprecipitation beads were incubated before the final elution with 3 nM of recombinant MARK2 in the kinase reaction buffer (50 mM HEPES, pH 7.5, 10 mM MgCl₂, 1 mM EGTA, 0.01% Brij-35) in the absence (control) or presence of 1 mM ATP for 1 h at 30°C. After that each reaction, beads were spun and the supernatant collected. The beads were further washed once with gentle rotation for 45 min at 4°C and eluted as described above. Eluates and supernatants from the reaction were analyzed by immunoblot.

For blot overlay, His-tagged recombinant 14-3-3 proteins (α , β , δ , ζ , ϵ , η ; 1 μg of each protein) were added onto the casein-saturated blots and incubated overnight at 4°C. The overlay was extensively washed, and the membranes were processed as for a regular immunoblot with anti-His antibody followed by chemiluminescence detection. Quantification of immunoblot results was performed by using chemiluminescence densitometry with a VersaDoc (BioRad) gel scanner and Quantimet software.

In vitro phosphorylation and phosphopeptide mass spectrometry

Recombinant GST-tagged MED17 protein (1 μg ; Novus Biologicals) was incubated with 1 nM of recombinant MARK2 (Invitrogen

Life Technologies) in the kinase reaction buffer (50 mM HEPES, pH 7.5, 10 mM MgCl₂, 1 mM EGTA, 0.01% Brij-35) in the presence or absence (control) of 1 mM ATP. Reactions were incubated at 30°C for 1 h and terminated by the addition of Laemmli SDS sample dilution buffer. Proteins were separated by 10% SDS-PAGE and subsequently visualized by GelCode Blue Stain Reagent (Thermo Fisher Scientific). The protein bands corresponding to the recombinant GST-tagged MED17 protein molecular weight were excised from stained gel and submitted for PTM-Profilung plus (MSB-09) service to MS Bioworks. In short, samples were processed by in-gel digestion with trypsin using a ProGest robot (Digilab). Excised gel bands were washed with 25 mmol/l ammonium bicarbonate followed by acetonitrile and then reduced with 10 mM dithiothreitol at 60°C followed by alkylation with 50 mmol/l iodoacetamide at room temperature, digested with trypsin (Promega) at 37°C for 4 h, and finally quenched with formic acid. Each digested sample was analyzed by nano LC/MS/MS (liquid chromatography-mass spectrometry) with a Proxeon EASY-nLC 1000 HPLC (high-performance liquid chromatography) system interfaced to a Thermo Fisher Q Exactive mass spectrometer. The mass spectrometer was operated in data-dependent mode, with MS and MS/MS performed in the Orbitrap at 70,000 and 17,500 FWHM (full width at half maximum) resolution, respectively. Mascot DAT files were parsed into the Scaffold software for validation and filtering and to create a non-redundant list per sample. Scaffold results were exported as mzIdentML and imported into Scaffold PTM in order to assign site localization probabilities using A-score (Beausoleil et al., 2006) A minimum localization probability filter of 50% was applied.

Animals and RNAseq

Animal work was performed in compliance with an internal animal care and use committee protocol. Characterization of the Prkci^{fllox/fllox} \times Vill-CRE mice was described before (intestinal epithelium PKC ζ / λ -deficient mice) (Forteza et al., 2016). Cryopreserved sperm has been deposited at the MMRRCC National Network (University of California, Davis, #042275). At the time of the experiments described here the mouse line had been kept in endogamic conditions for >20 generations. Breeders with Vill-CRE (-) genotypes were kept within the colony to obtain Prkci^{fllox/fllox} control animals. Control and knockout mice were cohoused.

The protocol to obtain RNA from Caco-2 cells for RNAseq studies was described above. Mouse intestine was extracted from Prkci^{fllox/fllox} Vill-CRE^{-/-} (control) and conditional PKC ζ / λ -deficient mice (Prkci^{fllox/fllox} Vill-CRE⁺). Three washes were performed using PBS supplemented with 10 mM glucose, 30 mM EDTA to remove debris and mucus. Following washes, each segment of intestine was loaded with a solution of PBS with glucose/EDTA and 0.5 mM DTT and clamped for 20 min. Intestinal lumens were then carefully drained by releasing one clamp into a sample tube. After a 1-min spin-down, RNase inhibitor (Qiagen, Germantown, MD) was immediately added to the pellet. Total RNA was extracted using 1 ml TRIzol Reagent and vigorously homogenized several times using 3 ml syringes (needles 18G11/2 and 20G11/2). Samples were then incubated at RT to permit complete dissociation of the nucleoprotein complex before adding chloroform (0.2 ml/ml phenol). Total RNA was then precipitated with isopropanol from the aqueous phase followed by 10 min centrifugation, 12,000 $\times g$ at 4°C. Pellets were washed with 75% ethanol, centrifuged for 5 min at 7500 $\times g$, air dried and finally resuspended in RNase-free water. All RNA samples were submitted to DNase Treatment and Removal Reagents following manufacturer's instructions (Ambion, Life Technologies). RNA samples were then stored at -80°C before being

processed for RNAseq by the Center for Genome Technology, University of Miami Miller School of Medicine. RNAs were extracted from epithelial cell-enriched mucosal scraps as described before (Forteza *et al.*, 2016) and submitted for poly-A selection and Illumina NextSeq/NovaSeq NGS technology. Results were filtered to exclude low count readings (<10 counts) and for statistical significance.

Statistics

Statistical significance for Gaussian variables was estimated by Student's *t* test. Specifically, this was used for qPCR data using Δ CT values (Yuan *et al.*, 2006), not fold differences, which were used for graphical purposes only. For RNAseq data, statistical significance of the differences was calculated using EdgeR or Illumina software. For transcript enrichment PANTHER software was used (<http://geneontology.org/>) for Biological Processes. For non-Gaussian variables, such as ratios, we used a nonparametric Kruskal–Wallis test.

ACKNOWLEDGMENTS

We thank Sanjoy Bhattacharya for advice with mass spectrometry and help to interpret data. This work was supported by National Institutes of Health (NIH) grant 1R01GM127953 to P.J.S. and a Research Development grant from Nova Southeastern University to A.M. The mass spectrometry facility was funded by NIH grant 2P30EY014801.

REFERENCES

- Beausoleil SA, Villen J, Gerber SA, Rush J, Gygi SP (2006). A probability-based approach for high-throughput protein phosphorylation analysis and site localization. *Nat Biotechnol* 24, 1285–1292.
- Bessone S, Vidal F, Le Bouc Y, Epelbaum J, Bluet-Pajot MT, Darmon M (1999). EMK protein kinase-null mice: dwarfism and hypofertility associated with alterations in the somatotrope and prolactin pathways. *Dev Biol* 214, 87–101.
- Calcagno SR, Li S, Shahid MW, Wallace MB, Leitges M, Fields AP, Murray NR (2011). Protein kinase C iota in the intestinal epithelium protects against dextran sodium sulfate-induced colitis. *Inflamm Bowel Dis* 17, 1685–1697.
- Capaldo CT, Farkas AE, Hilgarth RS, Krug SM, Wolf MF, Benedik JK, Fromm M, Koval M, Parkos C, Nusrat A (2014). Proinflammatory cytokine-induced tight junction remodeling through dynamic self-assembly of claudins. *Mol Biol Cell* 25, 2710–2719.
- Capaldo CT, Nusrat A (2009). Cytokine regulation of tight junctions. *Biochim Biophys Acta* 1788, 864–871.
- Cartón-García F, Overeem AW, Nieto R, Bazzocco S, Dopeso H, Macaya I, Bilic J, Landolfi S, Hernandez-Losa J, Schwartz S, *et al.* (2015). Myo5b knockout mice as a model of microvillus inclusion disease. *Sci Rep* 5, 12312.
- Chen M, Liang J, Ji H, Yang Z, Altília S, Hu B, Schronce A, McDermott MSJ, Schools GP, Lim CU, *et al.* (2017). CDK8/19 Mediator kinases potentiate induction of transcription by NF-kappaB. *Proc Natl Acad Sci USA* 114, 10208–10213.
- Cohen D, Rodriguez-Boulan E, Musch A (2004). Par-1 promotes a hepatic mode of apical protein trafficking in MDCK cells. *Proc Natl Acad Sci USA* 101, 13792–13797.
- Dequiedt F, Martin M, Von Blume J, Vertommen D, Lecomte E, Mari N, Heinen MF, Bachmann M, Twizere JC, Huang MC, *et al.* (2006). New role for hPar-1 kinases EMK and C-TAK1 in regulating localization and activity of class IIa histone deacetylases. *Mol Cell Biol* 26, 7086–7102.
- DiBona VL, Zhu W, Shah MK, Rafalia A, Ben Cheikh H, Crockett DP, Zhang H (2019). Loss of Par1b/MARK2 primes microglia during brain development and enhances their sensitivity to injury. *J Neuroinflammation* 16, 11.
- Drewes G, Ebneth A, Preuss U, Mandelkow EM, Mandelkow E (1997). MARK, a novel family of protein kinases that phosphorylate microtubule-associated proteins and trigger microtubule disruption. *Cell* 89, 297–308.
- Elbert M, Cohen D, Musch A (2006). PAR1b promotes cell-cell adhesion and inhibits dishevelled-mediated transformation of Madin-Darby canine kidney cells. *Mol Biol Cell* 17, 3345–3355.
- Forteza R, Figueroa Y, Mashukova A, Dulam V, Salas PJ (2016). Conditional knockout of polarity complex (atypical) PKC*iota* reveals an anti-inflammatory function mediated by NF-kappaB. *Mol Biol Cell* 27, 2186–2197.
- Forteza R, Wald FA, Mashukova A, Kozhekbaeva Z, Salas PJ (2013). Par-complex aPKC and Par3 cross-talk with innate immunity NF-kappaB pathway in epithelial cells. *Biol Open* 2, 1264–1269.
- Ganot P, Zoccola D, Tambutte E, Voolstra CR, Aranda M, Allemand D, Tambutte S (2015). Structural molecular components of septate junctions in cnidarians point to the origin of epithelial junctions in eukaryotes. *Mol Biol Evol* 32, 44–62.
- Garcia-Hernandez V, Quiros M, Nusrat A (2017). Intestinal epithelial claudins: expression and regulation in homeostasis and inflammation. *Ann NY Acad Sci* 1397, 66–79.
- Gilmore TD, Wolenski FS (2012). NF-kappaB: where did it come from and why? *Immunol Rev* 246, 14–35.
- Grasset E, Pinto M, Dussaux E, Zweibaum A, Desjeux JF (1984). Epithelial properties of human colonic carcinoma cell line Caco-2: electrical parameters. *Am J Physiol* 247, C260–C267.
- Hayashi K, Yonemura S, Matsui T, Tsukita S (1999). Immunofluorescence detection of ezrin/radixin/moesin (ERM) proteins with their carboxyl-terminal threonine phosphorylated in cultured cells and tissues. *J Cell Sci* 112 (Pt 8), 1149–1158.
- Hubaux R, Thu KL, Vucic EA, Pikor LA, Kung SH, Martinez VD, Mosslemi M, Becker-Santos DD, Gazdar AF, Lam S, Lam WL (2015). Microtubule affinity-regulating kinase 2 is associated with DNA damage response and cisplatin resistance in non-small cell lung cancer. *Int J Cancer* 137, 2072–2082.
- Hueso M, Beltran V, Moreso F, Ciriero E, Fulladosa X, Grinyo JM, Seron D, Navarro E (2004). Splicing alterations in human renal allografts: detection of a new splice variant of protein kinase Par1/Emk1 whose expression is associated with an increase of inflammation in protocol biopsies of transplanted patients. *Biochim Biophys Acta* 1689, 58–65.
- Hurov JB, Stappenbeck TS, Zmasek CM, White LS, Ranganath SH, Russell JH, Chan AC, Murphy KM, Piwnicka-Worms H (2001). Immune system dysfunction and autoimmune disease in mice lacking Emk (Par-1) protein kinase. *Mol Cell Biol* 21, 3206–3219.
- Hurov JB, Watkins JL, Piwnicka-Worms H (2004). Atypical PKC phosphorylates PAR-1 kinases to regulate localization and activity. *Curr Biol* 14, 736–741.
- Johnson C, Crowther S, Stafford MJ, Campbell DG, Toth R, MacKintosh C (2010). Bioinformatic and experimental survey of 14-3-3-binding sites. *Biochem J* 427, 69–78.
- Kemphues KJ, Priess JR, Morton DG, Cheng NS (1988). Identification of genes required for cytoplasmic localization in early *C. elegans* embryos. *Cell* 52, 311–320.
- Kim GH, Oh GS, Yoon J, Lee GG, Lee KU, Kim SW (2015). Hepatic TRAP80 selectively regulates lipogenic activity of liver X receptor. *J Clin Invest* 125, 183–193.
- Koch S, Nusrat A (2012). The life and death of epithelia during inflammation: lessons learned from the gut. *Annu Rev Pathol* 7, 35–60.
- Lam LT, Davis RE, Pierce J, Hepperle M, Xu Y, Hottelet M, Nong Y, Wen D, Adams J, Dang L, Staudt LM (2005). Small molecule inhibitors of IkkappaB kinase are selectively toxic for subgroups of diffuse large B-cell lymphoma defined by gene expression profiling. *Clin Cancer Res* 11, 28–40.
- Lennerz JK, Hurov JB, White LS, Lewandowski KT, Prior JL, Planer GJ, Gereau RW 4th, Piwnicka-Worms D, Schmidt RE, Piwnicka-Worms H (2010). Loss of Par-1a/MARK3/C-TAK1 kinase leads to reduced adiposity, resistance to hepatic steatosis, and defective gluconeogenesis. *Mol Cell Biol* 30, 5043–5056.
- Lin J, Hou KK, Piwnicka-Worms H, Shaw AS (2009). The polarity protein Par1b/EMK/MARK2 regulates T cell receptor-induced microtubule-organizing center polarization. *J Immunol* 183, 1215–1221.
- Livak KJ, Schmittgen TD (2001). Analysis of relative gene expression data using real-time quantitative PCR and the 2(-Delta Delta C(T)) method. *Methods* 25, 402–408.
- Lorentz CA, Liang Z, Meng M, Chen CW, Yoseph BP, Breed ER, Mittal R, Klingensmith NJ, Farris AB, Burd EM, *et al.* (2017). Myosin light chain kinase knockout improves gut barrier function and confers a survival advantage in polymicrobial sepsis. *Mol Med* 23, 155–165.
- Lung HL, Kan R, Chau WY, Man OY, Mak NK, Fong CH, Shuen WH, Tsao SW, Lung ML (2019). The anti-tumor function of the IKK inhibitor PS1145 and high levels of p65 and KLF4 are associated with the drug resistance in nasopharyngeal carcinoma cells. *Sci Rep* 9, 12064.
- Macara IG (2004). Par proteins: partners in polarization. *Curr Biol* 14, R160–R162.

- Mashukova A, Oriolo AS, Wald FA, Casanova ML, Kroger C, Magin TM, Omary MB, Salas PJ (2009). Rescue of atypical protein kinase C in epithelia by the cytoskeleton and Hsp70 family chaperones. *J Cell Sci* 122, 2491–2503.
- Mashukova A, Wald FA, Salas PJ (2011). Tumor necrosis factor alpha and inflammation disrupt the polarity complex in intestinal epithelial cells by a posttranslational mechanism. *Mol Cell Biol* 31, 756–765.
- Matenia D, Hempp C, Timm T, Eikhof A, Mandelkow EM (2012). Microtubule affinity-regulating kinase 2 (MARK2) turns on phosphatase and tensin homolog (PTEN)-induced kinase 1 (PINK1) at Thr-313, a mutation site in Parkinson disease: effects on mitochondrial transport. *J Biol Chem* 287, 8174–8186.
- Naar AM, Beaurang PA, Zhou S, Abraham S, Solomon W, Tjian R (1999). Composite co-activator ARC mediates chromatin-directed transcriptional activation. *Nature* 398, 828–832.
- Nakanishi Y, Duran A, L'Hermitte A, Shelton PM, Nakanishi N, Reina-Campos M, Huang J, Soldevila F, Baaten BJJ, Tauriello DVF, et al. (2018). Simultaneous loss of both atypical protein kinase C genes in the intestinal epithelium drives serrated intestinal cancer by impairing immunosurveillance. *Immunity* 49, 1132–1147.e1137.
- Nighot M, Rawat M, Al-Sadi R, Castillo EF, Nighot P, Ma TY (2019). Lipopolysaccharide-induced increase in intestinal permeability is mediated by TAK-1 activation of IKK and MLCK/MYLK gene. *Am J Pathol* 189, 797–812.
- Nozawa K, Schneider TR, Cramer P (2017). Core Mediator structure at 3.4 Å extends model of transcription initiation complex. *Nature* 545, 248–251.
- Olszak T, Neves JF, Dowds CM, Baker K, Glickman J, Davidson NO, Lin CS, Jobin C, Brand S, Sotlar K, et al. (2014). Protective mucosal immunity mediated by epithelial CD1d and IL-10. *Nature* 509, 497–502.
- Owen HR, Quadroni M, Bienvenut W, Buerki C, Hottiger MO (2005). Identification of novel and cell type enriched cofactors of the transcription activation domain of RelA (p65 NF-kappaB). *J Proteome Res* 4, 1381–1390.
- Park JM, Kim JM, Kim LK, Kim SN, Kim-Ha J, Kim JH, Kim YJ (2003). Signal-induced transcriptional activation by Dif requires the dTRAP80 mediator module. *Mol Cell Biol* 23, 1358–1367.
- Platanitis E, Decker T (2018). Regulatory networks involving STATs, IRFs, and NFkappaB in inflammation. *Front Immunol* 9, 2542.
- Salinas-Saavedra M, Stephenson TQ, Dunn CW, Martindale MQ (2015). Par system components are asymmetrically localized in ectodermal epithelia, but not during early development in the sea anemone *Nematostella vectensis*. *Evodevo* 6, 20.
- Sato Y, Akitsu M, Amano Y, Yamashita K, Ide M, Shimada K, Yamashita A, Hirano H, Arakawa N, Maki T, et al. (2013). The novel PAR-1-binding protein MTCL1 has crucial roles in organizing microtubules in polarizing epithelial cells. *J Cell Sci* 126, 4671–4683.
- Soutourina J (2019). Mammalian mediator as a functional link between enhancers and promoters. *Cell* 178, 1036–1038.
- Sturm A, Baumgart DC, d'Heureuse JH, Hotz A, Wiedenmann B, Dignass AU (2005). CXCL8 modulates human intestinal epithelial cells through a CXCR1 dependent pathway. *Cytokine* 29, 42–48.
- Suzuki A, Hirata M, Kamimura K, Maniwa R, Yamanaka T, Mizuno K, Kishikawa M, Hirose H, Amano Y, Izumi N, et al. (2004). aPKC acts upstream of PAR-1b in both the establishment and maintenance of mammalian epithelial polarity. *Curr Biol* 14, 1425–1435.
- Suzuki A, Ohno S (2006). The PAR-aPKC system: lessons in polarity. *J Cell Sci* 119, 979–987.
- Timm T, von Kries JP, Li X, Zempel H, Mandelkow E, Mandelkow EM (2011). Microtubule affinity regulating kinase activity in living neurons was examined by a genetically encoded fluorescence resonance energy transfer/fluorescence lifetime imaging-based biosensor: inhibitors with therapeutic potential. *J Biol Chem* 286, 41711–41722.
- Tremblay E, Auclair J, Delvin E, Levy E, Menard D, Pshezhetsky AV, Rivard N, Seidman EG, Sinnott D, Vachon PH, Beaulieu JF (2006). Gene expression profiles of normal proliferating and differentiating human intestinal epithelial cells: a comparison with the Caco-2 cell model. *J Cell Biochem* 99, 1175–1186.
- van Essen D, Engst B, Natoli G, Sacconi S (2009). Two modes of transcriptional activation at native promoters by NF-kappaB p65. *PLoS Biol* 7, e73.
- Wald FA, Forteza R, Diwadkar-Watkins R, Mashukova A, Duncan R, Abreu MT, Salas PJ (2011). Aberrant expression of the polarity complex atypical PKC and non-muscle myosin IIA in active and inactive inflammatory bowel disease. *Virchows Arch* 459, 331–338.
- Watkins JL, Lewandowski KT, Meek SE, Storz P, Tokar A, Piwnicka-Worms H (2008). Phosphorylation of the Par-1 polarity kinase by protein kinase D regulates 14-3-3 binding and membrane association. *Proc Natl Acad Sci USA* 105, 18378–18383.
- Xue J, Thomas L, Tahmasbi M, Valdez A, Dominguez Rieg JA, Fenton RA, Rieg T (2020). An inducible intestinal epithelial cell-specific NHE3 knockout mouse model mimicking congenital sodium diarrhea. *Clin Sci (Lond)* 134, 941–953.
- Yang SK, Eckmann L, Panja A, Kagnoff MF (1997). Differential and regulated expression of C-X-C, C-C, and C-chemokines by human colon epithelial cells. *Gastroenterology* 113, 1214–1223.
- Yang Y, Feng R, Wang YZ, Sun HW, Zou QM, Li HB (2020). Toll-like receptors: triggers of regulated cell death and promising targets for cancer therapy. *Immunol Lett* 223, 1–9.
- Yemelyanov A, Gasparian A, Lindholm P, Dang L, Pierce JW, Kisseljev F, Karseladze A, Budunova I (2006). Effects of IKK inhibitor PS1145 on NF-kappaB function, proliferation, apoptosis and invasion activity in prostate carcinoma cells. *Oncogene* 25, 387–398.
- Yuan JS, Reed A, Chen F, Stewart CN Jr (2006). Statistical analysis of real-time PCR data. *BMC Bioinformatics* 7, 85.